

International Journal of Modern Physics D
 © World Scientific Publishing Company

HALO MODELS IN MODIFIED GRAVITY THEORIES WITH SELF-ACCELERATED EXPANSION

TATSUYA NARIKAWA

*Department of Physical Science, Hiroshima University, Higashi-Hiroshima 739-8526, Japan
 narikawa@theo.phys.sci.hiroshima-u.ac.jp*

RAMPEI KIMURA

rampei@theo.phys.sci.hiroshima-u.ac.jp

TATSUNOSUKE YANO

yano@theo.phys.sci.hiroshima-u.ac.jp

KAZUHIRO YAMAMOTO

kazuhiro@hiroshima-u.ac.jp

We investigate the structure of halos in the sDGP (self-accelerating branch of the Dvali-Gabadadze-Porrati braneworld gravity) model and the galileon modified gravity model on the basis of the static and spherically symmetric solutions of the collisionless Boltzmann equation, which reduce to the singular isothermal sphere model and the King model in the limit of Newtonian gravity. The common feature of these halos is that the density of a halo in the outer region is larger (smaller) in the sDGP (galileon) model, respectively, in comparison with Newtonian gravity. This comes from the suppression (enhancement) of the effective gravity at large distance in the sDGP (galileon) model, respectively. However, the difference between these modified gravity models and Newtonian gravity only appears outside the halo due to the Vainshtein mechanism, which makes it difficult to distinguish between them. We also discuss the case in which the halo density profile is fixed independently of the gravity model for comparison between our results and previous work.

Keywords: cosmology, galaxies, halos

1. Introduction

Motivated from the discovery of the cosmic accelerated expansion of the universe^{1,2}, it is becoming important to test the nature of gravity on the cosmological scales. This is because the nature of gravity might be deeply rooted to the cosmic accelerated expansion (e.g., Refs. 3, 4, 5). In general, it is very challenging to construct a modified gravity (MG) theory that is consistent with observations. In comparison with the varieties of viable dark energy models to explain the accelerated expansion of the universe, many modified gravity models are ruled out by cosmological observations (e.g., Refs. 3, 4, 5, 6, 7).

For example, one of the most popular modified gravity models is the Dvali-Gavabadze-Porrati (DGP) model^{8,9}. The DGP model is described in the context of the braneworld scenario, which consists of a 3+1-dimensional brane embedded in a 5-dimensional bulk. This model has an interesting phenomenology and yields two branches of the Friedmann equation, which are a self-accelerating branch (sDGP) and a normal branch (nDGP). In the sDGP model, the expansion of the universe self-accelerates at late times without a cosmological constant nor spatial curvature, while the nDGP model needs to add a stress-energy component with negative pressure on the brane to be consistent with cosmological observations. Unfortunately, the sDGP model inevitably give rise to a ghost mode^{10,11,12}. Moreover, the sDGP model is disfavored by the cosmological observations^{13,14,15}.

Inspired by the decoupling limit of the DGP model, the galileon gravity theory has been studied as a possible alternative to large distance modification of gravity (e.g., Refs. 16, 17, 18, 19, 20, 21, 22, 23, 24, 25, 26, 27, 28, 29). This theory introduces a scalar field with the kinetic term with the "wrong" sign and the self-interaction term $(\partial\phi)^2\Box\phi$, which is invariant under the Galilean shift symmetry $\partial_\mu\phi \rightarrow \partial_\mu\phi + b_\mu$ in the Minkowski space-time, which keeps equation of motion at the second order differential equation. Although the Lagrangian no longer satisfies the Galilean shift symmetry in a curved spacetime, the field equation of the galileon field remains a second order differential equation, and the galileon field admits the self-accelerating solution in a FRW universe without a ghost instability.

The other notable feature of these modified gravity models is the Vainshtein mechanism, which allows the modification of gravity to recover general relativity around a high density region³⁰. Thanks to the Vainshtein mechanism, these models evade the solar system constraint. It is worth examining whether or not the effect of modification of gravity on the nonlinear scales and the structure of the halo of galaxy or galaxy cluster might be useful as a clue to test these modified gravity theory. Recently, several researchers have investigated such a possibility of testing these modified gravity models on the scales of galaxy or galaxy cluster^{31,32,33,34,35}. In the present paper, we focus our investigation on the structure of a halo in the sDGP model and the galileon model by constructing numerical solutions that correspond to the singular isothermal sphere (SIS) and the King model in the limit of Newtonian gravity.

The structure of this paper is as follows. In Sec. 2, we first give a brief review of the sDGP model and the galileon model. Then, we give basic formulas for our halo models in the sDGP model and the galileon model. In Sec. 3, our numerical results of the halo models are demonstrated. In Sec. 4, we investigate the case with a different approach for the halo modeling, in which the halo density profile is fixed independently of the gravity model for comparison between our results and previous work³¹. Sec. 5 is devoted to summary and conclusions. Throughout this paper, we use units in which the speed of light equals unity, and we follow the metric convention $(-, +, +, +)$. We use the reduce Planck mass M_{Pl} , which is defined by $M_{\text{Pl}} = 1/\sqrt{8\pi G}$ with Newton's gravitational constant G . We adopt the Hubble

constant $H_0 = 100 \text{ hkm/s/Mpc}$ with $h = 0.7$ and the matter density parameter at present $\Omega_0 = 0.28$.

2. Basic Formulas

2.1. Modified gravity models

The Dvali-Gabadadze-Porrati model consists of a spatially three-dimensional brane in a 4+1 dimensional (5D) Minkowski bulk. The action is^{8,9}

$$S = \frac{M_5^3}{2} \int d^5x \sqrt{-g_5} R_5 + \int d^4x \sqrt{-g} \left(\frac{M_{\text{Pl}}^2}{2} R + \mathcal{L}_m \right), \quad (1)$$

where M_5 (M_{Pl}) is the Planck mass in the 5 (4) dimensional spacetime, g_5 (g) and R_5 (R) are the determinant and the Ricci scalar of the 5 (4) dimensional metric, respectively, and \mathcal{L}_m stands for the matter Lagrangian. The two Planck masses M_5 and M_{Pl} can be related via length scale, the crossover scale $r_c \equiv M_{\text{Pl}}^2/2M_5^3$, which must be fine-tuned to be the present-day horizon scales in order to modify gravity only at late times. In this model, the Friedmann equation has two branches. One corresponds to the self-accelerating solution called sDGP, which contains a ghost-like instability. Although the other solution called nDGP does not suffer from a ghost instability, the cosmological constant is needed to drive the cosmic acceleration. In the present paper, we consider the self-accelerating branch of the DGP model. During matter domination and beyond, the modified Friedmann equation in the sDGP model is¹⁶

$$\frac{H(a)}{H_0} = \frac{1 - \Omega_0}{2} + \sqrt{\frac{\Omega_0}{a^3} + \frac{(1 - \Omega_0)^2}{4}}, \quad (2)$$

where a is the scale factor, and the matter density parameter is related to the crossover scale by $r_c = 1/(1 - \Omega_0)H_0$. Note that the modification of the law of gravity in the nDGP model is qualitatively similar to that in the galileon model. Therefore, our results in the galileon model can be applied to the nDGP model.

On the other hand, the galileon model is characterized by a scalar field with the self-interaction whose Lagrangian is invariant under the Galilean shift symmetry in the Minkowski spacetime^{18,19}. We consider the galileon model in a curved spacetime, which is minimally coupled to gravity, with the action^{24,25},

$$S = \int d^4x \sqrt{-g} \left[\frac{M_{\text{Pl}}^2}{2} R + K(X) - G(X) \square \phi + \mathcal{L}_m \right], \quad (3)$$

where R is the Ricci scalar, $X = -g^{\mu\nu} \nabla_\mu \phi \nabla_\nu \phi / 2$, $\square \phi = g^{\mu\nu} \nabla_\mu \nabla_\nu \phi$, \mathcal{L}_m is the matter Lagrangian, and $K(X)$ and $G(X)$ is an arbitrary function of X . For simplicity, we consider the following functions, $K(X) = -X$ and $G(X) = (r_c^2/M_{\text{Pl}})X$, where r_c is the model parameter. This model admits a late-time de-Sitter attractor in a flat FRW universe. The solution along this attractor can remarkably simplify the modified Friedmann equation, and the background evolution during the matter dominated era can be regarded as the Einstein de-Sitter universe. Besides, this

4 *T. Narikawa, R. Kimura, T. Yano, K. Yamamoto*

model is not plagued by ghost instability in contrast to the sDGP model. In the present paper, we consider the attractor solution. Then, the modified Friedmann equation on the attractor can be written as

$$\left(\frac{H(a)}{H_0}\right)^2 = \frac{1}{2} \left[\Omega_0 a^{-3} + \sqrt{(\Omega_0 a^{-3})^2 + 4(1 - \Omega_0)} \right]. \quad (4)$$

The parameter r_c is related with the cosmological parameters through the relation, $r_c = 1/(54(1 - \Omega_0))^{1/4} H_0^{-1}$.

Extended models of the galileon model have been proposed^{24,29}. In Ref. 29, the model with $G(X) = M_{\text{Pl}}(r_c^2/M_{\text{Pl}}^2)^n X^n$ is considered, and it is demonstrated that this model reduces to the cosmological constant model for n equal to infinity. Observational constraints on this model is also investigated, focusing on the constraints from the Ia supernovae (SN) observations and the cosmic microwave background (CMB) distance observation, as well as from the large scale structure of the luminous red galaxies in the sloan digital sky survey data release 7. The model with $n = 1$ is disfavored by the constraints from the SN and CMB observations, however, the model with higher n can be consistent with the observations. In the present paper, we consider the halo models of the galileon model with $n = 1$, however, the result is almost same as those with higher n at a quantitative level.

2.2. Perturbation equations in the static approximation

In this subsection, we summarize basic perturbation equations for gravity and the brane bending mode in the sDGP model and the galileon field on small scales, assuming the spherically symmetric and static system. For convenience, we choose the Newtonian gauge, which is given by

$$ds^2 = -(1 + 2\Psi)dt^2 + a^2(t)(1 + 2\Phi)\delta_{ij}dx^i dx^j, \quad (5)$$

where $a(t)$ is the scale factor, but we set $a(t) = 1$ in the expressions below, for simplicity. Following Refs. 10 and 36 for the DGP model, and Refs. 21 and 29 for the galileon model, within the subhorizon scales with the quasi-static approximation, we have the following perturbed equations,

$$\Delta\Phi = -4\pi G\rho + \xi\Delta\varphi, \quad (6)$$

$$\Phi + \Psi = -\alpha\varphi, \quad (7)$$

and

$$\Delta\varphi + \lambda^2(\varphi_{,ij}\varphi^{,ij} - (\Delta\varphi)^2) = -4\pi G\zeta\rho, \quad (8)$$

where $\varphi(x)$ denotes the brane bending mode and the perturbation of the galileon field defined by $\phi(t, x) = \phi(t)(1 + \varphi(x))$, the Laplace operator Δ represents the differentiation with respect to physical space-coordinates, ρ is the matter density.

Here, α , ξ , ζ , λ^2 and β are determined by the background evolution as follows:

$$\alpha = -1, \quad \xi = \frac{1}{2}, \quad \zeta = -\frac{2}{3\beta}, \quad \lambda^2 = -\frac{r_c^2}{3\beta}, \quad \beta = 1 - 2Hr_c \left(1 + \frac{\dot{H}}{3H^2}\right), \quad (9)$$

for the sDGP model^{10,36}, and

$$\begin{aligned} \alpha &= 0, \quad \xi = 4\pi G G_X \dot{\phi}^2 \phi, \quad \zeta = \frac{G_X \dot{\phi}^2}{\beta \phi}, \quad \lambda^2 = \frac{G_X \phi}{\beta}, \\ \beta &= -1 + 2G_X(\ddot{\phi} + 2H\dot{\phi}) - 4\pi G G_X^2 \dot{\phi}^4, \end{aligned} \quad (10)$$

for the galileon model, where we defined $G_X = \partial G(X)/\partial X$. For the galileon model, it is useful to rewrite the combinations $\xi\zeta$ and $\lambda^2\zeta$ in terms of the matter density parameter $\Omega_m = \rho_m(a)/3M_{\text{Pl}}^2 H^2(a)$,

$$\xi\zeta = \frac{(1 - \Omega_m)(2 - \Omega_m)}{\Omega_m(5 - \Omega_m)}, \quad \lambda^2\zeta = \left(\frac{2 - \Omega_m}{H\Omega_m(5 - \Omega_m)}\right)^2, \quad (11)$$

which is derived along the attractor solution (see e.g., Ref. 29).

In the spherically symmetric case, Eqs. (6), (7) and (8) reduce to

$$\frac{d\Psi}{dr} = \frac{GM(r)}{r^2} - (\alpha + \xi)\frac{d\varphi}{dr}, \quad (12)$$

$$\frac{d\varphi}{dr} = \frac{r}{4\lambda^2} \left(1 - \sqrt{1 + \frac{8G\lambda^2\zeta M(r)}{r^3}}\right), \quad (13)$$

where we define the enclosed mass $M(r) = 4\pi \int_0^r dr' r'^2 \rho(r')$. The influence of φ is determined by the second term in the square root in Eq. (13), which is characterized by the so-called Vainshtein radius, which we defined by

$$r_V = [8G\lambda^2\zeta M(r_V)]^{1/3}. \quad (14)$$

On scales smaller than the Vainshtein radius $r \ll r_V$, Eq. (13) gives $d\varphi/dr = -\sqrt{G\zeta M(r)/2\lambda^2 r} \ll GM(r)/r^2$. Therefore, the law of gravity in the Vainshtein limit reduces to Newtonian gravity,

$$\frac{d\Psi}{dr} \simeq \frac{GM(r)}{r^2}. \quad (15)$$

On scales larger than the Vainshtein radius $r \gg r_V$, Eq. (13) gives $d\varphi/dr = -G\zeta M(r)/r^2$. Thus, the modification of gravity at large distance becomes

$$\frac{d\Psi}{dr} \simeq \frac{G_{\text{eff}} M(r)}{r^2}, \quad (16)$$

where $G_{\text{eff}} = G(1 + (\alpha + \xi)\zeta)$ is the effective gravitational constant in the linearized limit. G_{eff}/G is always less than unity in the sDGP model, while G_{eff}/G is always larger than unity in the galileon model (also in the nDGP model).

6 *T. Narikawa, R. Kimura, T. Yano, K. Yamamoto*

2.3. Solution of Boltzmann equation

Next, let us consider the equation that the matter component obeys. Since the distribution of the matter is determined through the gravitational potential Ψ , the matter follows the usual collisionless Boltzmann equation. The static solution of the Boltzmann equation can be obtained by the Jean's theorem³⁷. We neglect the effect of time-dependent quantities in the modified Poisson equation (6) and the field equation (8), which might leads to the time-evolution of the effective gravitational constant. However, these time-dependent quantities evolve on cosmological time scales. Therefore, we can assume this effect can be neglected when considering the static solution of a halo.

In the present paper, we consider the singular isothermal sphere (SIS) model and the King model (see e.g., Ref. 37). The distribution function is given by

$$f(\mathcal{E}) = \frac{\rho_1}{(2\pi\sigma^2)^{3/2}} e^{\mathcal{E}/\sigma^2}, \quad (17)$$

for the SIS model, and

$$f(\mathcal{E}) = \begin{cases} \frac{\rho_1}{(2\pi\sigma^2)^{3/2}} (e^{\mathcal{E}/\sigma^2} - 1) & \mathcal{E} > 0, \\ 0 & \mathcal{E} \leq 0, \end{cases} \quad (18)$$

for the King model, respectively, where ρ_1 is a constant, $\mathcal{E} = -\Psi - s^2/2$, s is velocity, and σ is velocity dispersion. By integrating the distribution function over all velocities, we have the formula for the density,

$$\rho = \rho_1 e^{-\Psi/\sigma^2}, \quad (19)$$

for the SIS model, and

$$\rho = \rho_1 \left[e^{-\Psi/\sigma^2} \operatorname{erf} \left(\sqrt{\frac{-\Psi}{\sigma^2}} \right) - \sqrt{\frac{-4\Psi}{\pi\sigma^2}} \left(1 - \frac{2\Psi}{3\sigma^2} \right) \right], \quad (20)$$

for the King model, respectively, where $\operatorname{erf}(x)$ is the error function defined by $\operatorname{erf}(x) = (2/\sqrt{\pi}) \int_0^x e^{-t^2} dt$.

The basic equations for a halo are (12), (13) with (19) for the SIS model, but with (20) for the King model. These equations are numerically solved in the next section. In the case of Newtonian gravity, the solutions are well known³⁷. Especially, the solution of the SIS model is written in the simple analytic form, $\rho(r) = \sigma^2/2\pi Gr^2$.

3. Numerical results

3.1. Singular isothermal sphere (SIS) model

Now, we are ready to solve Eqs. (12), (13), and (19) to find the density profile of the SIS halo in the sDGP model and the galileon model. Figure 1 shows the density of the SIS halo divided by that of Newtonian gravity $\rho_{\text{GR}}(r)$, as a function of the radius r , where $\rho_{\text{GR}}(r) = \sigma^2/2\pi Gr^2$. The left panel is the sDGP model, while the right

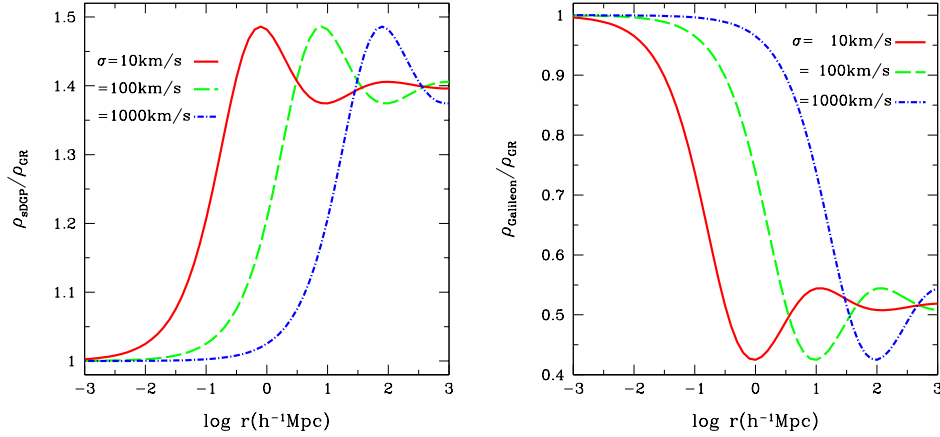


Fig. 1. The left panel is the ratio of the density of the SIS halo in the sDGP model to that of Newtonian gravity, as a function of radius r . Here, we adopted the velocity dispersion $\sigma = 10\text{km/s}$ (solid curve), $\sigma = 100\text{km/s}$ (dashed curve), and $\sigma = 1000\text{km/s}$ (dot-dashed curve), respectively. The right panel is the same as the left panel, but in the galileon model.

panel is the galileon model. Each curve corresponds to the velocity dispersion $\sigma = 10\text{km/s}$ (solid curve), $\sigma = 100\text{km/s}$ (dashed curve), and $\sigma = 1000\text{km/s}$ (dot-dashed curve), respectively. Here, we used the present values of the Hubble parameter and the matter density parameter in evaluating β , ζ , λ^2 , and ξ .

The density ratio, $\rho_{\text{MG}}/\rho_{\text{GR}}$, is almost unity at small radii r in both the models. This means that the central region is the same as that of Newtonian gravity. This is due to the Vainshtein mechanism. The difference appears as the radius r increases. We note that the density ratio finally approaches constant values as r becomes very large. Thus, there are two asymptotic regions, i.e., the Vainshtein limit $r \ll r_V$ and the linearized limit $r \gg r_V$.

In the Vainshtein limit $r \ll r_V$, from Eqs. (12), (13) and (19), we obtain the approximate density profile,

$$\rho_{\text{MG}}(r) \simeq \rho_{\text{GR}}(r) \exp \left(-\frac{(\alpha + \xi)\zeta}{\sqrt{\lambda^2 \zeta} \sigma} r \right). \quad (21)$$

Thus, the effect of modification of gravity is represented by the factor $(\alpha + \xi)\zeta/\sqrt{\lambda^2 \zeta} \sigma$. On the other hand, in the linearized limit $r \gg r_V$, Eqs. (16) and (19) give the approximate solution

$$\rho_{\text{MG}}(r \gg r_V) \simeq \frac{G}{G_{\text{eff}}} \rho_{\text{GR}}(r). \quad (22)$$

Thus, the density is enhanced (decreased) in the sDGP (galileon) model at large radii r , reflecting the behavior of $G/G_{\text{eff}} = 1/(1 + (\alpha + \xi)\zeta)$.

Let us estimate the Vainshtein radius r_V , which can be easily done by substituting the relation $M = 2\sigma^2 r_V / G$, extrapolated from Newtonian gravity, into Eq. (14).

8 *T. Narikawa, R. Kimura, T. Yano, K. Yamamoto*

Then, we have the approximate formula of the Vainshtein radius,

$$r_V \simeq 4\sqrt{\lambda^2 \zeta} \sigma. \quad (23)$$

This gives a good approximate expression. However, the exact solution of Eq. (14) gives a slightly different value from Eq. (23), due to the underestimation (overestimation) of the mass of the halo in the sDGP (galileon) model at $r \sim r_V$. Our numerical analysis of Eq. (14) shows that the following formula works,

$$r_V \simeq 2.5 \left(\frac{\sigma}{100 \text{km/s}} \right) h^{-1} \text{Mpc}, \quad (24)$$

for the sDGP model, and

$$r_V \simeq 4.2 \left(\frac{\sigma}{100 \text{km/s}} \right) h^{-1} \text{Mpc}, \quad (25)$$

for the galileon model, respectively.

We next consider the circular speed of a test particle in a circular orbit at radius r , which is given by equating the gravitational force with the centrifugal force

$$v^2(r) = r \frac{d\Psi}{dr}. \quad (26)$$

Figure 2 shows the ratio of circular speed in the modified gravity model to that in Newtonian gravity, $v_{\text{MG}}^2/v_{\text{GR}}^2$, as a function of radius $r(h^{-1}\text{Mpc})$. Note that the circular speed in the SIS halo model satisfies $v_{\text{GR}}^2 = 2\sigma^2$ in Newtonian gravity. The left (right) panel of Fig. 2 shows the sDGP (galileon) model. Each curve corresponds to the various velocity dispersion $\sigma = 10\text{km/s}$ (solid curve), $\sigma = 100\text{km/s}$ (dashed curve), and $\sigma = 1000\text{km/s}$ (dot-dashed curve), respectively.

Inside the Vainshtein radius $r \ll r_V$, we have $v_{\text{MG}}^2 \simeq v_{\text{GR}}^2$ due to the Vainshtein mechanism. However, v_{MG}^2 becomes to deviate from v_{GR}^2 as r becomes larger. The oscillatory feature appears at $r \sim r_V$. We suppose that the nonlinear structure of basic equations plays an important role in the oscillatory behavior around $r \sim r_V$. Finally, v_{MG}^2 approaches v_{GR}^2 again at large radii r in both models. This behavior can be understood by considering the asymptotic solution of the density profile. Namely, in the limit $r \gg r_V$, using Eq. (16), we obtain

$$v_{\text{MG}}^2(r \gg r_V) \simeq \frac{G_{\text{eff}} M_{\text{MG}}(r)}{r} \simeq v_{\text{GR}}^2(r), \quad (27)$$

with the enclosed mass $M_{\text{MG}}(r) = 4\pi \int_0^r dr' r'^2 \rho_{\text{MG}}(r')$. Since the density of a halo in this limit is given by Eq. (22), the effective gravitational constant is canceled out in Eq. (27) and the circular speed of a test particle in these modified gravity models is equal to that of Newtonian gravity. The characteristic behavior at $r \sim r_V$ appears well outside galaxies or galaxy clusters. Therefore, this effect of modification of gravity will be hard to be detected.

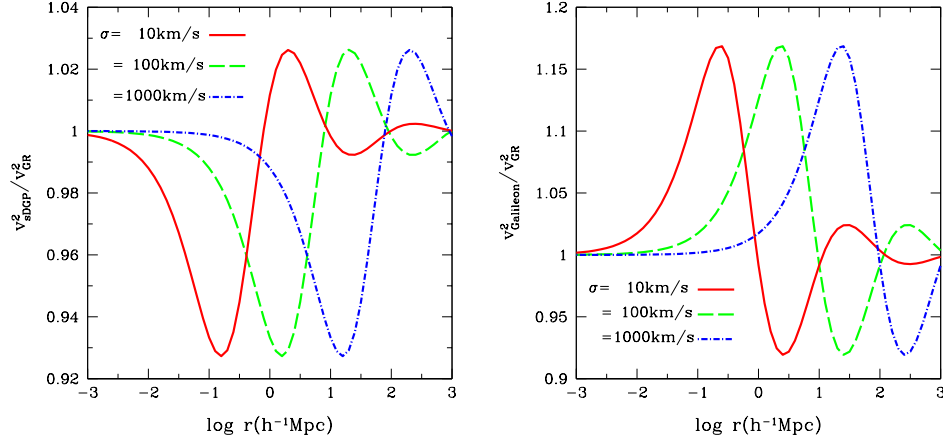


Fig. 2. The left panel is the ratio of the circular speed of a test particle for the SIS model in the sDGP model to that in Newtonian gravity, as a function of radius $r(h^{-1}\text{Mpc})$. Here, we adopted the velocity dispersion $\sigma = 10\text{km/s}$ (solid curve), $\sigma = 100\text{km/s}$ (dashed curve), and $\sigma = 1000\text{km/s}$ (dot-dashed curve), respectively. The right panel is the same as the left panel, but in the galileon model.

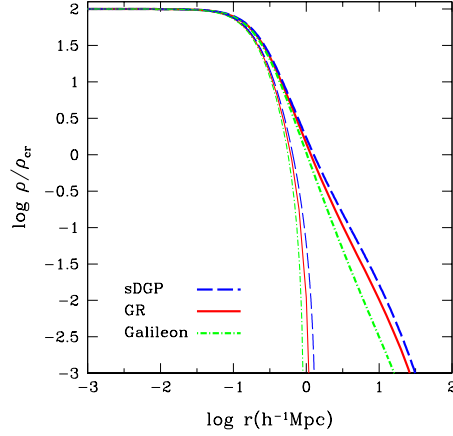


Fig. 3. The density profile of the King model as a function of radius $r(h^{-1}\text{Mpc})$. The density is normalized by the critical density at present. The thick curves represent the density profile with the central potential $\Psi_0 = -12\sigma^2$, while the thin curves represent the density profile with $\Psi_0 = -3\sigma^2$. The dashed, solid, and dot-dashed curve correspond to the sDGP model, Newtonian gravity, and the galileon model, respectively. Here, the velocity dispersion is fixed as $\sigma = 100\text{km/s}$.

3.2. King model

The density profile of the King model can be obtained by solving Eqs. (12), (13) and (20). In Fig. 3, we show the density profile of the King model normalized by the

critical density at present, as a function of the radius, where the curves correspond to the sDGP model (dashed curve), Newtonian gravity (solid curve), and galileon model (dot-dashed curve), respectively. We adopted the values of the potential at the center, $\Psi_0 = -12\sigma^2$ (thick curves) and $\Psi_0 = -3\sigma^2$ (thin curves), respectively. Here, we set the velocity dispersion $\sigma = 100\text{km/s}$. In general, the halo density in the King model remains constant at small radii r , and becomes smaller as r increases.

In the King model, the density of a halo has a cut-off radius r_t , called the tidal radius, which is defined by $\Psi(r_t) = 0$. From Eq. (20), we may set $\rho = 0$ for $r \geq r_t$. Similar to the case of the SIS halo model, the density is enhanced (decreased) in the sDGP (galileon) model in the outer region of halo in comparison with that of Newtonian gravity, which explains the behavior of the density near the tidal radius in Fig. 3, depending on the models of gravity.

We define the total mass of a halo by $M_{\text{tot}} \equiv M(r_t)$. In the left panel of Fig. 4, we plot the tidal radius r_t as a function of central potential Ψ_0/σ^2 for the sDGP model (dashed curve), Newtonian gravity (solid curve), and the galileon model (dot-dashed curve), respectively. The right panel of Fig. 4 plots the total mass as a function of the central potential, Ψ_0/σ^2 , where each curve is the sDGP model (dashed curve), Newtonian gravity (solid curve), and the galileon model (dot-dashed curve), respectively. The total mass of the sDGP (galileon) model is larger (smaller) than that of Newtonian gravity. The difference of the total mass between the gravity models becomes larger as the absolute value of the central potential is larger.

In the left panel of Fig. 4, we also plot the Vainshtein radius r_V . The thin dashed curve and the thin dot-dashed curve represent the Vainshtein radius for the sDGP model and the galileon model, respectively. In the case $r_t < r_V$, the density profile at any radius is effectively described by Newtonian gravity, since all radii enclosing matter are inside the Vainshtein radius. In the limit of small central potential $|\Psi_0|/\sigma^2$, the tidal radius becomes very small, $r_t \ll r_V$. In this limit, therefore, the difference of the tidal radius between the gravity models becomes small. On the other hand, in the limit of large central potential $|\Psi_0|/\sigma^2$, the tidal radius becomes large, $r_t \gg r_V$. In the case $r_t > r_V$, the density profile in the outer region reflects the modification of gravity. Then, the difference of the tidal radius between the gravity models remains in the limit of $|\Psi_0|/\sigma^2 \gg 1$ or $r_t \gg r_V$. Let us now consider the question whether the gravity model can be distinguishable or not. Even for the case $r_t > r_V$, the difference in the density profile appears only in the outer region of a halo. Thus, the difference between those modified gravity theories and general relativity is small, and it will be difficult to be distinguished observationally.

4. Discussion

In Ref. 31, the author investigated the halos in the DGP modified gravity model with N-body simulations as well as analytic modeling of a halo similar to our investigation. Here, let us discuss the difference between the results in Ref. 31 and

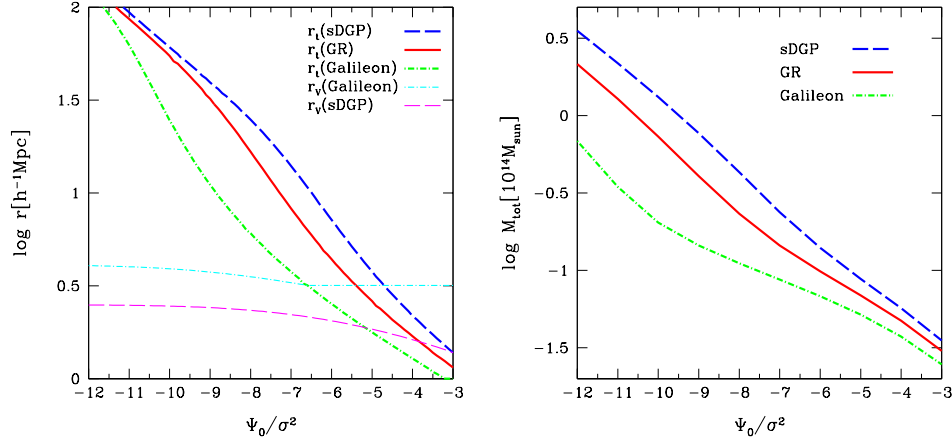


Fig. 4. The left panel plots the tidal radius (thick curves) and the Vainshtein radius (thin curves) of the King model as a function of Ψ_0/σ^2 . Each thick curve is the tidal radius in the sDGP model (thick curve), Newtonian gravity (solid curve), and galileon model (dot-dashed curve), respectively. The thin dashed (dot-dashed) curve is the Vainshtein radius in the sDGP (galileon) model, respectively. The right panel plots the total mass M_{tot} as a function of Ψ_0/σ^2 , for the sDGP (dashed curve), Newtonian gravity (solid curve), and galileon model (dot-dashed curve), respectively.

ours. The author in Ref. 31 has found that the square of the circular speed of a test particle is enhanced or decreased in outer region of a halo in proportion to G_{eff} . On the contrary, our result in the SIS model is different, which the circular speed in the outer region finally approaches the value in the inner region of a halo. The difference comes from the treatment of the dark matter component. In our analysis, we adopted the explicit formula for the distribution function for the dark matter component, which is evidently the solution of the Boltzmann equation. Thus, in our approach the same distribution function is assumed for the different gravity model, which results in the different density profiles, depending on the gravity models.

On the other hand, the author of Ref. 31 fixed the density profile of a halo independently of the gravity model, which has been suggested from N-body simulations. Following this method, the circular speed in a modified gravity model approaches that in Newtonian gravity multiplied by the factor G_{eff}/G in the limit of large radii. Fig. 5 shows the ratio of the circular speed of a test particle in the sDGP model and the galileon model to that in Newtonian gravity with fixing the density profile so as to be the SIS model, $\rho_{\text{MG}}(r) = \sigma^2/2\pi Gr^2$. In Fig. 5, we can see the similar feature of the circular speed in both the modified gravity models as that expected from Ref. 31.

Following Ref. 31, we next consider an Navarro-Frenk-White³⁸ (NFW) halo with mass M_{200} , defined as the mass contained with a radius R_{200} so that the average density within R_{200} is $200\bar{\rho}$, where $\bar{\rho}$ is the background density, and we used the concentration relation³⁹, $c = 9 \times (M/[3.2 \times 10^{12} M_{\odot}/h])^{-0.13}$. In this case, the virial

radius is written $R_{200} \simeq 1.0 \times (M_{200}/10^{14}M_{\odot})^{1/3} h^{-1}\text{Mpc}$, and the concentration is $c \simeq 6.0 \times (M_{200}/10^{14}M_{\odot})^{-0.13}$ (see, e.g., Ref. 31 for details). Fig. 6 shows the ratio of the circular speed in the modified gravity models to that in Newtonian gravity. Similar feature as that in Fig. 5 can be seen for the NFW halo. In Fig. 6, we choose the mass $M_{200} = 10^{13}M_{\odot}$ (solid curve), $10^{14}M_{\odot}$ (dashed curve), $10^{15}M_{\odot}$ (dot-dashed curve), which correspond to clusters. The effect of the modified gravity is significant in the outer region of a halo, but it is suppressed in the inner region because of the Vainshtein mechanism. For the NFW halo, the Vainshtein radius is estimated as

$$r_V \simeq 5.6 \left(\frac{M_{200}}{10^{14}M_{\odot}} \right)^{1/3} h^{-1}\text{Mpc}, \quad (28)$$

for the sDGP model, and

$$r_V \simeq 11 \left(\frac{M_{200}}{10^{14}M_{\odot}} \right)^{1/3} h^{-1}\text{Mpc}, \quad (29)$$

for the galileon model, respectively, from Eq. (14). The Vainshtein radius is large, but the Vainshtein mechanism does not completely hide the effect of the modification of gravity in the cluster. One can read that the circular speed is enhanced or decreased in comparison with Newtonian halo, e.g., at 10% level at the radius of a few $h^{-1}\text{Mpc}$ for $M_{200} = 10^{14}M_{\odot}$. If a good tracer of circular speed is available, there might be a possible chance to test the modified gravity effect in a halo, as discussed in Ref. 31.

5. Summary and conclusions

In this paper, we have investigated the structure of dark matter halos in the sDGP model and the galileon model by using the static and spherically symmetric solutions of the collisionless Boltzmann equation, which reduce to the SIS model and the King model in the limit of Newtonian gravity. We have obtained the solution of a halo in these modified gravity theories in a numerical manner. The density of the halo is the same as that in Newtonian gravity due to the Vainshtein mechanism well inside the Vainshtein radius $r \ll r_V$. We have found that the density in the sDGP (the galileon) model becomes larger (smaller) in the outer region of a halo, in comparison with that in Newtonian gravity, which comes from the suppression (enhancement) of the effective gravitational constant in the sDGP (galileon) model, respectively. In the SIS model, the density of the halo at large radii $r \gg r_V$ approaches the value of Newtonian gravity multiplied by a factor G/G_{eff} . The circular speed is also modified around $r \sim r_V$. However, the Vainshtein radius is $r_V \simeq 1 \sim 10\text{Mpc}$ for a typical galaxy and $r_V \simeq 10 \sim 100\text{Mpc}$ for a typical galaxy cluster. Therefore, it will be difficult to distinguish between these modified gravity theories by a measurement of a halo because the Vainshtein radius is large enough.

However, the above results rely on the assumption that the distribution function of the dark matter follows the simple explicit formula. For a comparison with the

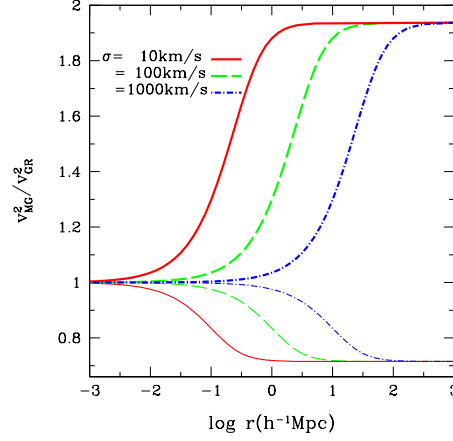


Fig. 5. The ratio of the circular speed of a test particle in the galileon model (thick curves) and the sDGP model (thin curves) to that in Newtonian gravity for the SIS model, as a function of radius $r(h^{-1}\text{Mpc})$, when the density profile of a halo is fixed so as to be the SIS model, $\rho_{\text{MG}}(r) = \sigma^2/2\pi Gr^2$. Here, we adopted the velocity dispersion $\sigma = 10\text{km/s}$ (solid curve), $\sigma = 100\text{km/s}$ (dashed curve), and $\sigma = 1000\text{km/s}$ (dot-dashed curve), respectively. For large r , this ratio approaches $G_{\text{eff}}/G = 1 + \xi\xi \simeq 1.94$ for the galileon model, and $G_{\text{eff}}/G = 1 + 1/(3\beta) \simeq 0.715$ for the sDGP model, respectively.

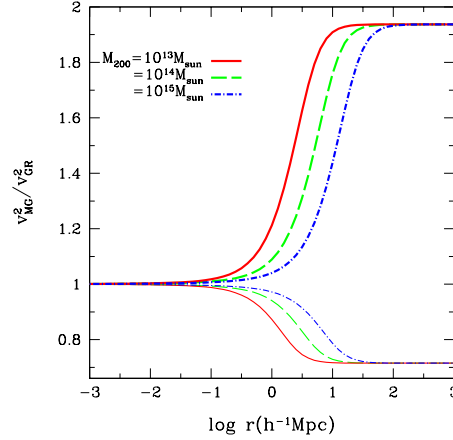


Fig. 6. The same as Fig. 5, but for the NFW halo. Here, we adopted the virial mass $M_{200} = 10^{13}M_{\odot}$ (solid curve), $10^{14}M_{\odot}$ (dashed curve), and $10^{15}M_{\odot}$ (dot-dashed curve), respectively. The asymptotic value of G_{eff}/G at large r is same as that in Fig. 5.

previous approach in Ref. 31, we investigated the effect of the modification of gravity with fixing the halo density profile independently of the gravity model. In this case, the circular speed is enhanced or decreased in the outer region of a halo depending

14 *T. Narikawa, R. Kimura, T. Yano, K. Yamamoto*

on the gravity model. In the case adopting the NFW profile as a model of a cluster halo, the Vainshtein radius is large. However, the Vainshtein mechanism does not completely hide the effect of the modification of gravity in the cluster. This might provide a possible chance that precise measurement of halo could be a probe of the modified gravity, as discussed in Ref. 31.

Acknowledgments

We thank anonymous referee for useful comments which helped improve the original manuscript. This work was supported by Japan Society for Promotion of Science (JSPS) Grants-in-Aid for Scientific Research (Nos. 21540270, 21244033). This work was also supported by JSPS Core-to-Core Program “International Research Network for Dark Energy”. TN and RA acknowledge support by a research assistant program of Hiroshima University. This work was supported in part by a Grant-in-Aid for JSPS Fellows (TN).

References

1. A. G. Riess et al., *Astron. J.* **116** (1998) 1009
2. S. Perlmutter et al., *Astropys. J.* **517** (1999) 565
3. R. Durrer, R. Maartens, arXiv:0811.4132
4. B. Jain and J. Khoury, *Annals of Physics* **325** (2010) 1479
5. S. Tsujikawa, *Lect. Notes Phys* **800** (2010) 99
6. E. J. Copeland, M. Sami and S. Tsujikawa, *Int. J. Mod. Phys. D* **15** (2006) 1753
7. L. Amendla and S. Tsujikawa, *Dark Energy: Theory and Observations* (Cambridge University Press, 2010)
8. G. R. Dvali, G. Gabadadze and M. Porrati, *Phys. Lett. B* **485** (2000) 208
9. C. Deffayet, *Phys. Lett. B* **502** (2001) 199
10. K. Koyama and R. Maartens, *JCAP* **01** (2006) 016
11. A. Nicolis and R. Rattazzi, *JHEP* **0406** (2004) 059
12. D. Goubnov, K. Koyama and S. Sibiryakov, *Phys. Rev. D* **73** (2006) 044016
13. M. Fairbairn and A. Goobar, *Phys. Lett. B* **642** (2006) 432
14. R. Maartens and E. Majerotto, *Phys. Rev. D* **74** (2006) 023004
15. Y. S. Song, I. Sawicki and W. Hu, *Phys. Rev. D* **75** (2007) 064003
16. C. Deffayet, G. R. Dvali and G. Gabadadze, *Phys. Rev. D* **65** (2002) 044023
17. M. A. Luty, M. Porrati and R. Rattazzi, *JHEP* **0309** (2003) 029
18. A. Nicolis, R. Rattazzi and E. Trincherini, *Phys. Rev. D* **79** (2009) 064036
19. C. Deffayet, G. Esposito-Farese and A. Vikman, *Phys. Rev. D* **79** (2009) 084003
20. N. Chow and J. Khoury, *Phys. Rev. D* **80** (2009) 024037
21. F. P. Silva and K. Koyama, *Phys. Rev. D* **80** (2009) 121301
22. T. Kobayashi, H. Tashiro and D. Suzuki, *Phys. Rev. D* **81** (2010) 063513
23. T. Kobayashi, *Phys. Rev. D* **81** 103533 (2010)
24. C. Deffayet, O. Pujolas, I. Sawicki and A. Vikman, *JCAP* **10** (2010) 026
25. T. Kobayashi, M. Yamaguchi and J. Yokoyama, *Phys. Rev. Lett.* **105** (2010) 231302
26. A. De Felice and S. Tsujikawa, arXiv:1008.4236
27. A. De Felice and S. Tsujikawa, *Phys. Rev. Lett.* **105** (2010) 111301
28. S. Nesseris, A. De Felice and S. Tsujikawa, *Phys. Rev. D* **82** (2010) 124054
29. R. Kimura and K. Yamamoto, *JCAP* **04** (2011) 025

30. A. I. Vainshtein, Phys. Lett. B **39** (1972) 393
31. F. Schmidt, Phys. Rev. D **81** (2010) 103002
32. M. Wyman, Phys. Rev. Lett. **106** (2011) 201102
33. K. Konno et al., Phys. Rev. D **78** (2008) 024037
34. L. A. Gergely et al., arXiv:1105.0159
35. P. Burikham and S. Panpanich, arXiv:1103.1198
36. K. Koyama and F. P. Silva, Phys. Rev. D **75** (2007) 084040
37. J. Binney and S. Tremain, *Galactic Dynamics* (Princeton University Press, 2008)
38. J. F. Navarro, C. S. Frenk and S. D. M. White, Astrophys. J. **490** (1997) 493
39. J. S. Bullock, et al., Mon. Not. R. Astron. Soc. **321** (2001) 559